Applied Catalysis B: Environmental 126 (2012) 306–314

Contents lists available at SciVerse ScienceDirect

Applied Catalysis B: Environmental

journal homepage: www.elsevier.com/locate/apcatb

Effect of support for Pt—Cu bimetallic catalysts synthesized by electron beam irradiation method on preferential CO oxidation

J. Kugai[a,*], T. Moriya[a], S. Seino[a], T. Nakagawa[a], Y. Ohkubo[a], H. Nitani[b], Y. Mizukoshi[c], T.A. Yamamoto[a]

[a] Graduate School of Engineering, Osaka University, 2-1 Yamadaoka, Suita, Osaka 565-0871, Japan
[b] Institute of Materials Structure Science (IMSS), High Energy Accelerator Research Organization (KEK), 1-1 Oho, Tsukuba, Ibaraki 305-0801, Japan
[c] Kansai Center for Industrial Materials Research, Institute for Materials Research, Tohoku University, 1-1 Gakuen-cho, Naka-ku, Sakai, Osaka 599-8531, Japan

ARTICLE INFO

Article history:
Received 21 May 2012
Received in revised form 14 July 2012
Accepted 25 July 2012
Available online 2 August 2012

Keywords:
Pt—Cu
Bimetallic catalyst
Preferential oxidation
CeO_2 support
Electron beam irradiation

ABSTRACT

Supported bimetallic catalysts have been shown to improve properties and catalytic performance of monometallic catalysts in various fuel conversion reactions. To investigate the effect of support on bimetallic Pt—Cu system, Pt—Cu supported on γ-Fe_2O_3 and CeO_2 were synthesized using electron beam irradiation method and preferential CO oxidation (PROX) performance was investigated in relation to structural and chemical properties of the catalysts. The difference in performance among the catalysts existed in both oxygen transport ability and selectivity. While oxygen transport ability was influenced by support property such as crystallite size (within the comparison among catalysts supported on CeO_2 and γ-Fe_2O_3), selectivity was rather influenced by support material which led to clear differences in reducibility, reduction degree of catalyst, and alloying extent of Pt—Cu. CeO_2-supported catalysts are unique in the view point that they were able to convert CO selectively in high CO conversion region compared to Fe_2O_3-supported catalyst. Pt—Cu with small CeO_2 crystallite maintained high O_2 conversion (high capacity for oxygen transport) in O_2-rich atmosphere in addition to high selectivity. Compared to monometallic Cu which lost its activity in the O_2-rich wet condition, or compared to monometallic Pt which exhibited poor selectivity, Pt—Cu realized both high activity and selectivity on CeO_2 of small crystallite size, leading to more than 99% of CO conversion at 100 °C. By modifying the structure, it was demonstrated that Pt—Cu/CeO_2 system can be improved to have low-temperature activity comparable to monometallic Pt while keeping high selectivity of the original Pt—Cu catalyst in the practical PROX condition.

1. Introduction

Preferential oxidation of carbon monoxide (PROX) is one of the critical reactions for hydrogen production for polymer electrolyte membrane fuel cell (PEMFC) since the anode catalyst is severely poisoned by ppm-order of CO in the H_2-rich fuel [1,2]. The poisoning is caused by CO strongly adsorbing on Pt surface through donating π-electron to d-orbital of platinum and backdonation of electron from platinum to anti-bonding orbital of CO. To avoid this, increasing reaction temperature is one of the solutions, but higher temperature causes low CO coverage, increasing the chance for H_2 adsorption and oxidation on the surface resulting in decrease of CO conversion [3]. Operating low temperature is another option which has an advantage in obtaining high selectivity for CO oxidation, but highly active catalyst is indispensable. In this sense, catalyst that has both activity at low temperature and selectivity at high temperature is desired to supply CO-free H_2 to fuel cell on real-time output demand.

In seeking catalyst to achieve such PROX performance, researchers have modified electronic structure of Pt combined with transition metals. Kotobuki et al. added Fe to Pt/mordenite to see significant enhancement in PROX activity and selectivity [4]. Oxygen pulse reaction on CO-preadsorbed catalyst revealed that Fe provides O_2 chemisorption sites for dual-site reaction pathway, otherwise O_2 chemisorption is inhibited by high CO coverage on active Pt sites. Similar enhancement was reported for Pt—Fe/Al_2O_3 by Liu et al. and it was attributed to partial coverage of Pt surface by Fe oxide to provide electron-rich Pt and O_2 chemisorption sites. Au/TiO_2 was also modified by Fe successfully to increase low temperature performance [5]. Cobalt-modified Pt/Al_2O_3 or Pt/SiO_2 was reported to be promising formulation for PROX. Yan et al. impregnated Co on Pt/Al_2O_3 and observed a drastic shift in light-off temperature with little change in selectivity [6]. Choi et al. prepared Pt—Co/SiO_2 by sol–gel method in which Co cations

* Corresponding author. Tel.: +81 6 6879 4454; fax: +81 6 6879 7886.
E-mail addresses: kugai@mit.eng.osaka-u.ac.jp (J. Kugai), t-moriya@mit.eng.osaka-u.ac.jp (T. Moriya), seino@mit.eng.osaka-u.ac.jp (S. Seino), nakagawa@mit.eng.osaka-u.ac.jp (T. Nakagawa), okubo@mit.eng.osaka-u.ac.jp (Y. Ohkubo), hiroaki.nitani@kek.jp (H. Nitani), mizukosi@imr.tohoku.ac.jp (Y. Mizukoshi), takao@mit.eng.osaka-u.ac.jp (T.A. Yamamoto).

0926-3373/$ – see front matter © 2012 Elsevier B.V. All rights reserved.
http://dx.doi.org/10.1016/j.apcatb.2012.07.028

selectively attached to Pt sites and stabilized Pt in a reduced state [7]. In intermetallic Pt—Co or Pt—Cu on SiO_2, the neighboring Co or Cu creates electron-deficient Pt to weaken CO adsorption and to accelerate O_2 adsorption [8]. Our group has studied copper-modification of Pt/Fe_2O_3 or Pt/CeO_2 using radiation-induced reduction method which is a unique one-pot aqueous-phase process to obtain supported bimetallic nanoparticles with uniform size and distribution in a matter of several seconds [9–11]. We found that Cu addition enhances oxygen transport and improves selectivity significantly.

While addition of transition metal can improve geometric, electronic structures, and catalytic performance, effect of support has not been much understood for these bimetallic catalysts. Each bimetallic formulation works only on specific support material. For instance, Pt—Fe has advantage over monometallic Pt on Al_2O_3, but not much on CeO_2 [11]. Similarly, Pt—Co can work on Al_2O_3 [6] or SiO_2 [7], but good performance on $Pt—Co/CeO_2$ has never been reported. Pt—Cu is also good on SiO_2 [8] or redox support such as CeO_2 [11], Fe_2O_3 [10], Nb_2O_5 [12], but $Pt—Cu/Al_2O_3$ performs worse than Pt/Al_2O_3 [12]. To help understanding of support effect in Pt—Cu system, in the present study, Pt—Cu on three redox supports, Fe_2O_3 and two CeO_2 from different sources, were synthesized by electron beam irradiation method and their PROX performances in various temperatures and O_2 partial pressures were compared in relation to their structural and chemical properties of catalyst. The advantages in bimetallic Pt—Cu over monometallic Pt or Cu supported on CeO_2 were also discussed.

2. Methods

The procedure for catalyst preparation is given elsewhere [9,13], so a brief description is given here. The aqueous precursor solution was prepared using $H_2PtCl_6{\cdot}6H_2O$ (99.9%, Wako), $CuSO_4{\cdot}5H_2O$ (99.9%, Wako). Powder of γ-Fe_2O_3 (NanoTek®, C. I. Kasei Co., 64 m^2/g of specific surface area, 27 nm of average crystallite size) or CeO_2 (NanoTek®, C. I. Kasei Co., 78 m^2/g, 24 nm, denoted as CeO_2(NT), or HSA20®, Anan Kasei Co., 140 m^2/g, 10 nm, denoted as CeO_2(HSA)) were dispersed in the solution. The concentration of chloroplatinic ion in the solution was 0.1 mM, that of copper ion was 0.1 mM or 0.9 mM, and the amount of support powder was adjusted to achieve 2.54 wt.% of platinum loading and 0.83 wt.% or 7.5 wt.% of copper loading in total catalyst weight basis. The catalysts synthesized by these recipes are denoted as "Pt10Cu10" and "Pt10Cu90", respectively. 2-propanol (Wako) was added to scavenge hydroxyl radical which is formed in the radiation-induced reduction process. The concentration of 2-propanol was 0.25 mol/L. The solution was well mixed and sealed in a polypropylene flask after argon bubbling to remove dissolved oxygen. It was then irradiated with 4.8 MeV electron beam for several seconds at room temperature (20 kGy). The irradiation with electron beam induces water radiolysis to generate hydrated electrons and radicals, which in turn reduce the ionic precursors to form nanoparticles deposited on the support by electrostatic force [14,15]. Indeed, the greenish or bluish color of the solution immediately turned blackish upon irradiation of electron beam. The product was filtrated, washed, and dried at 80 °C to obtain catalyst samples.

The chemical composition of the catalysts was analyzed by an inductively coupled plasma atomic emission spectrometry (ICP-AES; SHIMADZU, ICPS-7500). Crystallographic information on support and Pt—Cu species was obtained by an X-ray diffractometer (XRD; RIGAKU, RINT2100-Ultima with Cu Kα radiation). Temperature-programmed reduction (TPR) was performed on AutoChem II 2920 (Micromeritics). About 50 mg of catalyst was heated in 10%H_2/Ar flow from room temperature to 600 °C at 5 °C/min of ramp rate. Extended X-ray absorption fine structure (EXAFS) spectra were measured at the beam line NW10A of photon factory advanced ring (High Energy Accelerator Research Organization, Tsukuba, Japan) using fluorescence method. Pt L_3 edge absorption (11–13 keV) of as-made catalyst was analyzed using software Athena ver. 0.8.056.

Performance for preferential CO oxidation was tested using a fixed-bed flow reactor. About 50 mg of catalyst powder was packed in a glass tube reactor with 4 mm of inner diameter. The reactant gas mixture was 1% CO, 0.5% O_2, 67.2% H_2, N_2 balance (λ = 1 dry), or 1% CO, 0.7% O_2, 66% H_2, N_2 balance plus 10% H_2O (λ = 1.4 wet), or 1% CO, 1% O_2, 64% H_2, N_2 balance plus 10% H_2O (λ = 2 wet) where "λ" is defined as degree of O_2 excess from stoichiometry, i.e. twice of O_2/CO ratio in the feed. Water vapor was introduced by bubbling dry reactant gas mixture in the water adjusted to 46.1 °C and all gas lines were heated at around 100 °C. The total gas flow rate was 25 ml/min (dry gas) for all above conditions. The temperature was measured inside the oven containing the reactor tube. The product gases (CO, CO_2, O_2) in the effluent were quantified by gas chromatograph Varian 490 Micro GC equipped with dual channels, one with MS-5 A column and the other with Plot Q, and TCD detector for each column. CO conversion, O_2 conversion, and CO_2 selectivity were calculated as follows:

$$\text{CO conversion} = \left(\frac{1 - |\text{CO}|_{\text{out}}}{|\text{CO}|_{\text{in}}}\right) \times 100$$

$$\text{O}_2\text{conversion} = \left(\frac{1 - |\text{O}_2|_{\text{out}}}{|\text{O}_2|_{\text{in}}}\right) \times 100$$

$$\text{Selectivity} = \left(\frac{(\text{CO conversion}/\text{O}_2\text{conversion})}{\lambda}\right) \times 100$$

where $|CO|_{out}$, $|O_2|_{out}$, $|CO|_{in}$, $|O_2|_{in}$ are concentrations of CO, O_2 in outlet and those in inlet, respectively. The effluent was demoisturized at 0 °C before gas analysis.

3. Results and discussion

3.1. Characteristics of Pt—Cu/CeO_2 in preferential CO oxidation

Fig. 1 shows the results of PROX tests on Pt—M (M = second metal: Fe, Co, Cu) bimetallic catalysts supported on CeO_2 which were synthesized by radiolytic method. It has been shown in our previous study that $Pt—Cu/CeO_2$ is highly selective in PROX in wide temperature range [11] and the present results clarified difference of Pt—Cu from other Pt—M systems. Addition of Fe or Co did not change selectivity of monometallic Pt catalyst on CeO_2 and the light-off temperature was lowered by these metals instead. The enhanced light-off performance on Pt—M catalysts is consistent with literature. Pt—M supported on Al_2O_3 has been reported to be more active at low temperature compared to monometallic Pt, among which Pt—Co and Pt—Fe are distinguished, but the selectivity are similar to Pt at high temperature range [16]. Ko et al. have also shown that Pt—Co/YSZ (yttria-stabilized zirconia) shifted light-off temperature of Pt/YSZ by a matter of 50 °C though selectivity converged to certain value at high temperature [17]. Even Pt—Co core–shell structure obtained by calcination at 700 °C had 20–30 °C lower light-off temperature than Pt alone. The authors attributed it to oxygen vacancies on redox support in contact with Pt—Co nanoparticles. Regarding the enhanced light-off, Tanaka et al. have shown that Pt catalysts on carbon nanotube (CNT) containing Ni or Fe exhibit similar kinetic feature in PROX to FeO_x-added Pt/TiO_2 reported in their earlier study [18,19]. A reaction pathway via hydroxyl carbonyl or bicarbonate intermediates was proposed for improved activity at the low temperature region where the parent Pt/CNT or Pt/TiO_2 does not show activity. Regardless of

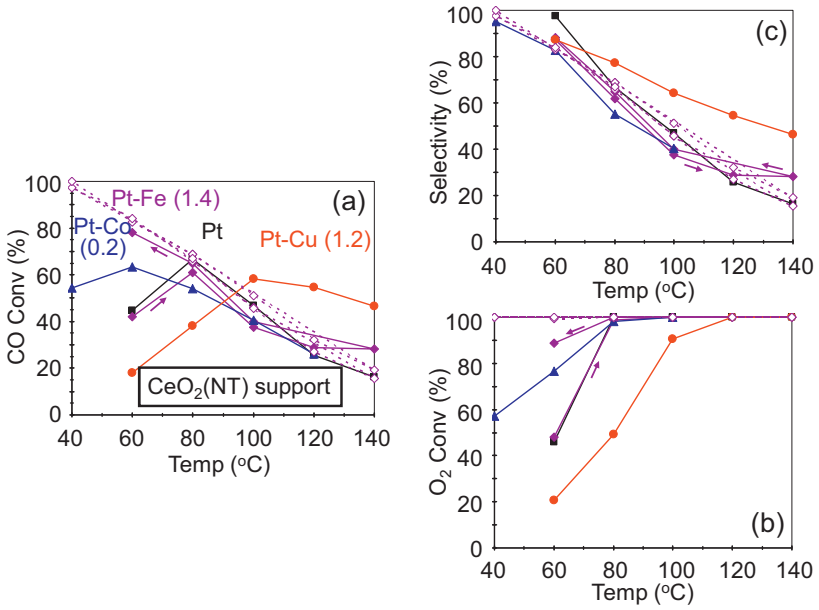

Fig. 1. Comparison of PROX performance on various CeO_2-supported Pt—M bimetallic catalysts synthesized by radiolytic method (M = transition metal). Filled square: monometallic Pt; filled triangle: Pt—Co; filled circle: Pt—Cu; filled diamond: Pt—Fe; open diamond: Pt—Fe (second test). Gas composition: 1% CO/0.5% O_2/67% H_2/N_2 balance, GHSV = ca. 25,000 h^{-1}. Inside parenthesis presents M/Pt molar ratio in catalyst measured by ICP. The concentrations of Pt and M source ions were both 0.1 mM. The light-off of first heating–cooling cycle on Pt—Fe was variable, but activity was constant after second cycle. Possibility of external mass transfer control can be eliminated.

mechanistic arguments, the enhancement of activity is mainly observable at lower temperature in these reports and selectivity at higher temperature has not been focused much. The present result shows that Cu addition inhibits the low-temperature light-off of monometallic Pt, which must be compensated by increase of O_2 addition, but it significantly improves selectivity. The selectivity curve along reaction temperature in fact showed milder decline on Pt—Cu/CeO_2 than other Pt—Fe or Pt—Co/CeO_2. The reaction characteristics of Pt—Cu/CeO_2 are thus different from other Pt—M/CeO_2 catalysts. In the following sections, we will further investigate the effect of support on Pt—Cu catalysts in PROX performance in relation to their structural and chemical properties.

3.2. Characterization of supported Pt—Cu catalysts

3.2.1. Catalyst composition

The compositions of catalysts synthesized by radiolytic method were measured by ICP and the results are summarized in Table 1. The low-Cu (Pt10Cu10) catalysts prepared from equimolar $PtCl_6^{2-}$ and Cu^{2+} precursors showed metal loading close to each target value, 2.5 wt.% for Pt and 0.83 wt.% for Cu in total weight basis. The metal loadings were thus well controlled for low-Cu samples. The high-Cu (Pt10Cu90) catalysts prepared from excess Cu^{2+} to $PtCl_6^{2-}$ showed Pt loading close to 2.5 wt.%, but the Cu loading was smaller than the target value, since a part of Cu^{2+} ion was left unreduced in the solution as reported in our previous paper [10,11]. Cu^{2+} is more difficult to reduce and copper is easily reoxidized even if it is produced [20]. The metal loadings of γ-Fe_2O_3-supported Pt10Cu90 sample were higher than the target values. Pt (3.1 wt.%) is 1.2 times higher and Cu (8.3 wt.%) was 1.1 times higher. The filtrate was brownish, so some of the iron oxide dissolved into the solution and the apparent metal loading increased. The reason has not been clarified yet. It seems iron oxide dissolution is sensitive to the temperature and ionic species in the solution. The influence of these synthesis parameters is under investigation.

Table 1
Catalyst composition measured by ICP.

Catalyst	Pt (wt.%)	Cu (wt.%)	$Cu/Pt_{catalyst}$ (mol/mol)
Pt10Cu90/γ-Fe_2O_3	3.1	8.3	8.2
Pt10Cu10/γ-Fe_2O_3	2.9	0.8	0.9
Pt10Cu90/CeO_2(HSA)	2.5	4.1	5.0
Pt10Cu10/CeO_2(HSA)	2.6	1.0	1.2
Pt10Cu90/CeO_2(NT)	2.5	4.1	5.4
Pt10Cu10/CeO_2(NT)	2.7	1.0	1.2

3.2.2. X-ray diffraction

Fig. 2(a) shows XRD patterns of low-Cu (Pt10C10) catalysts supported on γ-Fe_2O_3 and two CeO_2. From the peak width, the crystallite size of the supports was calculated using the following equation:

$$\tau = \frac{K\Lambda}{\beta \cos\theta} \quad (1)$$

where τ is crystallite size, K is the shape factor (0.9) which is an attribute of equipment, Λ is the wavelength of X-ray (1.54 Å for Cu-Kα), β is the line broadening at half the maximum intensity (FWHM), and θ is Bragg angle. The average crystallite size of support was 27 nm for γ-Fe_2O_3, 24 nm for CeO_2(NT), and 10 nm for CeO_2(HSA). In Fig. 2(b), magnification of XRD pattern between 35 and 45° of 2θ range was given. Broad diffraction peaks at 40–42° originates from Pt or Pt—Cu lattice of nanoparticles. The size of crystalline Pt—Cu phase was roughly estimated to be 4 nm using above Scherrer's equation (Eq. (1)), except the size of 5.3 nm for Pt10Cu90/γ-Fe_2O_3, as presented in Table 2. All the samples had diffraction peak at higher angle than pure Pt (39.8°), indicating that Pt is partially substituted by Cu and the lattice contracted, i.e. Pt formed alloy with Cu. For the catalysts with two CeO_2 supports, Pt(1 1 1) peaks appeared at similar 2θ angle, i.e. low-Cu (Pt10Cu10) samples had diffraction peak at around 41.1° and high-Cu (Pt10Cu90) samples had diffraction peak at around 41.5°. The γ-Fe_2O_3-supported catalysts had peaks at lower angle. Support thus influences extent of alloying between Pt and Cu possibly through interaction of Cu with support during electron beam irradiation. Crystalline CuO phase is also observable, supporting

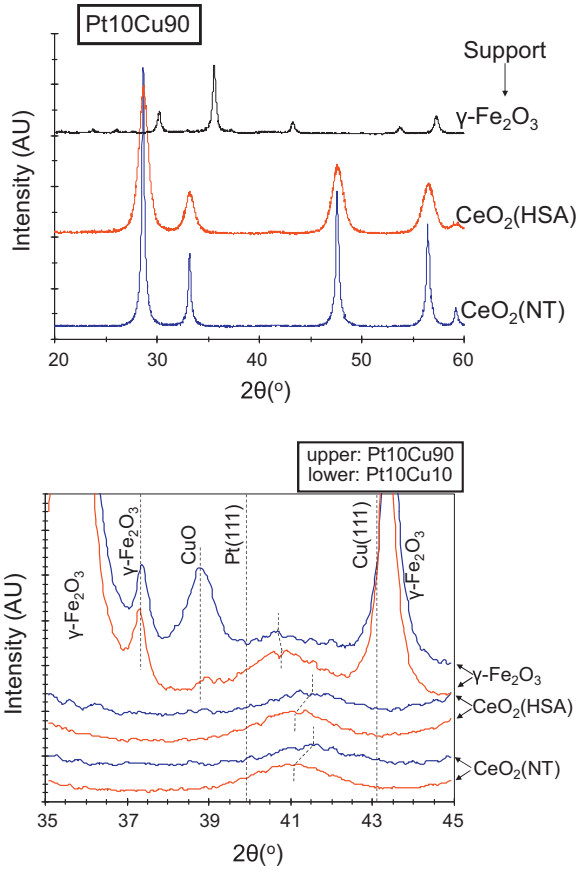

Fig. 2. X-ray diffraction patterns of Pt—Cu bimetallic catalysts with three different supports. (a) 20–60° of wide scan, (b) magnification of 35–45° of narrow scan.

that CuO is easily formed or stable in the presence of γ-Fe_2O_3 than CeO_2.

The lattice constant of Pt—Cu alloy was calculated using the following Bragg's equation:

$$d = \frac{\Lambda}{2\sin\theta} \quad (2)$$

where d is the spacing between the lattice planes, Λ is the wavelength of incident X-ray, and θ is the Bragg angle. Cu content in the alloy was further estimated from the peak shift by assuming Vegard's law that holds the lattice constant of alloy is proportional to the concentration of the constituents of alloy [21]. The estimated Cu content in Pt—Cu alloy (Cu/Pt_{alloy}) was much lower than the Cu content in catalyst ($Cu/Pt_{catalyst}$) measured by ICP (see Table 2 in comparison with Table 1). Cu/Pt_{alloy} was 0.5 against 1.2 of $Cu/Pt_{catalyst}$ for Pt10Cu10/CeO_2 and 0.7–0.8 against 5 for Pt10Cu90/CeO_2. The rest of Cu is amorphous or crystalline oxide segregated from Pt—Cu alloy as it was shown by CuO peak in XRD

Table 2
Pt—Cu alloy composition estimated from diffraction angle and size of Pt—Cu alloy crystallites calculated from XRD peak broadening.

Catalyst	Cu/Pt_{alloy}[a] (mol/mol)	Particle size (nm)
Pt10Cu90/γ-Fe_2O_3	0.32 ± 0.04	5.3
Pt10Cu10/γ-Fe_2O_3	0.39 ± 0.05	4.3
Pt10Cu90/CeO_2(HSA)	0.77 ± 0.10	3.9
Pt10Cu10/CeO_2(HSA)	0.49 ± 0.07	4.0
Pt10Cu90/CeO_2(NT)	0.81 ± 0.10	3.7
Pt10Cu10/CeO_2(NT)	0.50 ± 0.07	3.7

[a] Estimated from reading error of 1/10 of FWHM.

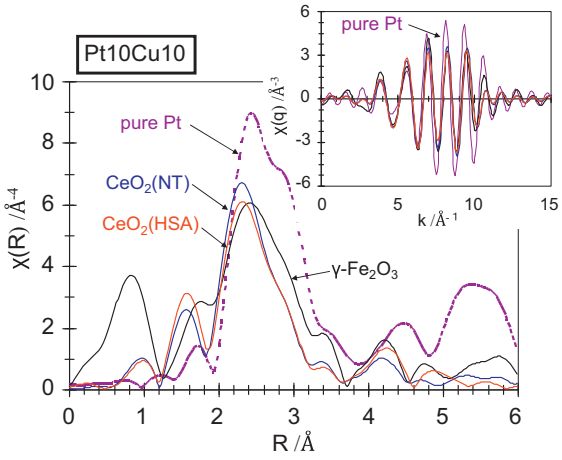

Fig. 3. Fourier transform of Pt L_3 edge EXAFS (k = 2.5–10.5 $Å^{-1}$) of Pt10Cu10 catalysts. The inset shows reverse Fourier transform of 1–3 Å of R range.

(Fig. 2(b)) and our previous XANES study [10]. The temperature-programmed reduction (TPR) spectra in Section 3.2.4 also prove the presence of CuO species.

3.2.3. EXAFS study

Fig. 3 shows Fourier transform of Pt L_3 edge EXAFS spectra. Compared with Pt metal, there was little Pt—Pt scattering from second shell (over 4 Å) for all the samples. The reverse Fourier transform (see inset in Fig. 3) clearly shows different oscillation for Pt metal from those of Pt—Cu samples, which can be interpreted as difference in bond distance due to Pt—Cu bonds shorter than Pt—Pt bonds. In comparison among the three Pt—Cu catalysts, radial distribution was different between CeO_2-supported and Fe_2O_3-supported catalysts. The bond distance of Pt—Pt (Pt—Cu) is slightly larger on Pt10Cu10/Fe_2O_3 than Pt10Cu10/CeO_2, which is also reflected in difference in oscillation above 10 $Å^{-1}$ in the reverse Fourier transform. This is also consistent with lower extent of Cu incorporation into Pt lattice as it was shown by XRD (Fig. 2(b)). The EXAFS data support that coordination environment of Pt or structure of Pt—Cu nanoparticles is similar, but extent of alloying is different.

3.2.4. Temperature-programmed reduction

Fig. 4(a) shows TPR spectra of catalysts with the three different supports. H_2 uptake was calculated from each peak area based on the peak area of known amount of pure CuO (see Table 3). The temperature and extent of reduction strongly depended on the support material and properties. The H_2 uptake at 100–200 °C is related to the reduction of CuO and support surface in its periphery [22–24]. In fact, the absence of reduction peak at this temperature range for pure CeO_2(NT) and the presence of a distinct peak for both Pt—Cu/CeO_2(NT) and Cu/CeO_2(NT) show that the low-temperature reduction peak primarily originates from reduction of CuO (see Fig. 4(b)). If we assume that all of copper exists as CuO, H_2 uptake by CuO reduction would be at most 0.13–0.16 mmol/g for Pt10Cu10 samples and 0.65 mmol/g for Pt10Cu90/CeO_2 and 1.04 mmol/g for Pt10Cu90/Fe_2O_3, but the actual H_2 uptake at 100–200 °C was larger in most of the cases, suggesting significant reduction of support accompanies. The low-temperature H_2 uptake on Pt10Cu10/CeO_2(NT) was negligible, suggesting that large portion of copper is present as Pt—Cu alloy or easily reduced below ambient temperature [11]. It is possible that copper interacts with platinum more than it interacts with CeO_2(NT) support. The low-temperature H_2 uptake on Pt10Cu90/CeO_2(NT) was however comparable to that for Pt10Cu90/CeO_2(HSA). High-Cu samples have substantial amount of CuO species that interacts with

Table 3
H_2 uptake in TPR measurement.

Catalyst	Low-temperature H_2 uptake		High-temperature H_2 uptake	
	Peak temp. (°C)	H_2 uptake (mmol/g-cat.)	Peak temp. (°C)	H_2 uptake (mmol/g-cat.)
Pt10Cu90/γ-Fe_2O_3	105	1.98	518	14.3
Pt10Cu10/γ-Fe_2O_3	92	1.44	524	16.1
Pt10Cu90/CeO_2(HSA)	128	0.86	422	0.75
Pt10Cu10/CeO_2(HSA)	106	0.72	420	0.69
Pt10Cu90/CeO_2(NT)	146	0.87	406	0.38
Pt10Cu10/CeO_2(NT)	110	0.05	~410	0.30

Carrier gas: 10%H_2/Ar 30 ml/min(STP), catalyst weight: 50 mg H_2 uptake was calculated based on H_2 uptake of pure CuO.

support. The H_2 uptake for Fe_2O_3-suppoted Pt—Cu was more than twice larger than those of CeO_2-supported Pt—Cu, indicating reduction of γ-Fe_2O_3 surface is deeper than that of CeO_2 surface. The reduction temperature increased in the order of Pt—Cu/γ-Fe_2O_3 < Pt—Cu/CeO_2(HSA) < Pt—Cu/CeO_2(NT), which is inverse to the H_2 uptake (peak area). These results show that the strength of interaction between CuO and support is in the order: γ-Fe_2O_3 > CeO_2(HSA) > CeO_2(NT). Literature also reports that higher reducibility of CuO reflects larger interaction with support [25].

The peak above 350 °C is attributed to reduction of support surface and partially its bulk. H_2 uptake and reduction temperature were dependent on support material rather than Cu loading. H_2 uptake by CeO_2 surface reduction to Ce_2O_3 is theoretically calculated to be 0.66 mmol-H_2/g for CeO_2(NT) and 1.2 mmol-H_2/g for CeO_2(HSA) respectively if 1×10^{15} atoms/cm^2 was assumed for surface Ce density. H_2 uptake for Pt—Cu/CeO_2(HSA) was 0.7–0.8 mmol/g and Pt—Cu/CeO_2(NT) was 0.3–0.4 mmol/g, both of which are roughly 50–70% of the theoretical H_2 uptake. The rest would be reduced together with Pt and Cu species below 350 °C. Therefore, CeO_2 can be reduced only to Ce(III) state. The γ-Fe_2O_3-supported catalysts had much larger peak. The H_2 uptake, 14–16 mmol/g, is close to the theoretical value for bulk reduction of γ-Fe_2O_3 to metallic Fe, 18 mmol/g. Thus, γ-Fe_2O_3 is completely reduced to metallic state by 600 °C. The deeper reduction of Fe_2O_3 than CeO_2 indicates that an irreversible change in structure and valence state could occur easily in the course of catalytic reaction.

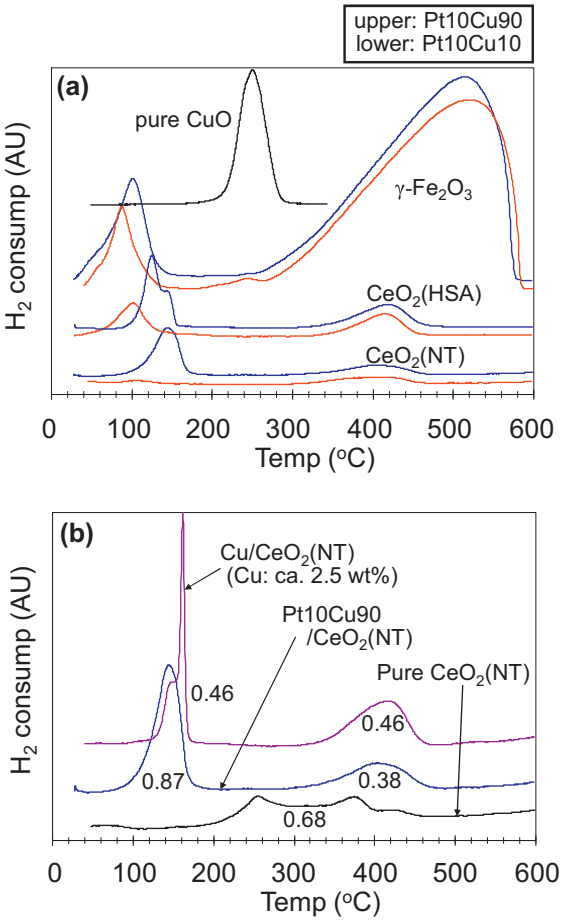

Fig. 4. (a) TPR spectra of CeO_2-supported and Fe_2O_3-supported Pt—Cu bimetallic catalysts. Carrier gas: 10% H_2/Ar balance, 30 ml/min (STP). Catalyst weight: 50 mg. (b) TPR spectra of pure Pt—Cu/CeO_2, Cu/CeO_2, and pure CeO_2. Carrier gas: 10% H_2/Ar balance, 30 ml/min (STP). Sample weight: 50 mg. The numbers beside the peaks are H_2 uptake in the unit of mmol/g.

3.3. Catalytic tests

3.3.1. Effect of support

Fig. 5 shows PROX performance between the three low-Cu (Pt10Cu10) catalysts with different supports. All the catalysts showed similar activity pattern where CO conversion reached the maximum at 100 °C. The order of activity was Pt—Cu/CeO_2(HSA) > Pt—Cu/CeO_2(NT) > Pt—Cu/γ-Fe_2O_3. At 60 °C, the three catalysts showed about 20% of CO conversion, indicating the support effect is not remarkable at this temperature. As temperature increases, the difference in CO conversion and selectivity became larger while difference in O_2 conversion was not as large. Thus, activity strongly reflected selectivity. The slope in Fig. 5(c), or temperature dependency of selectivity, in fact, was mildest for Pt—Cu/CeO_2(HSA) and steepest for Pt—Cu/γ-Fe_2O_3. We have reported in our previous paper that copper addition significantly improves selectivity towards CO oxidation [11]. The present results show that selectivity depends not only on copper loading, but also on support material. Note that the activity of pure support was negligible, e.g. CeO_2(NT) showed only 2% of O_2 conversion at 160 °C.

In Fig. 6, the comparison was made in the oxidative condition where twice of O_2 partial pressure and 10% moisture were added. Although the order of activity stayed same, activity and selectivity trends differed from stoichiometric O_2/CO condition. Comparing Fig. 6(b) with Fig. 5(b), O_2 conversion was maintained on the catalyst with Pt—Cu/CeO_2(HSA) while it was not on Pt—Cu/CeO_2(NT) and Pt—Cu/γ-Fe_2O_3. This suggests that small crystallite size of CeO_2(HSA) provides higher capacity to adsorb/transport oxygen than the other two catalysts to keep up with the increased O_2 supply. As a result, CeO_2(HSA) showed higher CO conversion at 60–80 °C while the other two exhibited similar CO conversions to those in the stoichiometric O_2/CO condition. Oxygen adsorption/transport ability of support becomes apparent when gas phase O_2 is abundant, which suggests that support has impacts not only on selectivity, but also oxygen adsorption/transport.

The function of CeO_2 as oxygen carrier was demonstrated by Gorte's group. They observed two kinetic regions in CO oxidation reaction in excess CO to O_2 on Rh/CeO_2 catalyst, one with inverse first-order in CO (competitive Langmuir–Hinshelwood pathway) and another with zeroth-order in CO (non-competitive

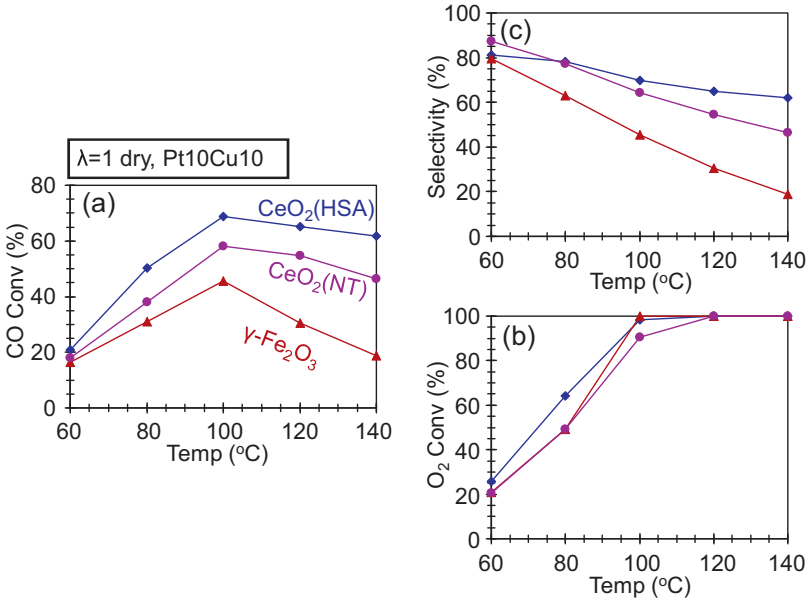

Fig. 5. Effect of support on PROX performance in stoichiometric O_2/CO condition. Diamond: Pt—Cu/CeO_2(HSA); circle: Pt—Cu/CeO_2(NT); triangle: Pt—Cu/γ-Fe_2O_3, gas composition: 1% CO/0.5% O_2/67% H_2/N_2 balance, GHSV = ca. 25,000 h^{-1}.

redox pathway) [26]. According to their report, when CO partial pressure was increased, CO coverage increased and the competing O_2 activation on metallic sites decreased. At certain point, the O_2 activation on metallic sites fell below O_2 activation via redox of CeO_2 to attain kinetics independent of CO partial pressure. The present study demonstrated that such oxygen transport capacity inherent to support material can also be seen in O_2-rich condition.

Selectivity was also dependent on support in O_2-rich atmosphere. While selectivity of Fe_2O_3-supported catalyst monotonically decreased along temperature, that of CeO_2-supported catalyst was less dependent on temperature. Even over 100 °C, selectivity was maintained at around 50% up to 140 °C resulting in CO conversion kept over 90%. The discontinuity (the large selectivity drop) between 80 °C and 100 °C is not clear at this point. Since this is observed only in high O_2 condition, λ = 2, but not in low O_2 condition, λ = 1 or 1.4 (see Fig. 7(c)), selectivity could be ruled by CO coverage (or competitive chemisorptions of CO and H_2) below 80 °C while it could be ruled by competitive oxidation of CO and H_2 above 100 °C. In any case, selectivity strongly reflects support material in O_2-rich atmosphere.

For comparison, reaction characteristics on monometallic Pt catalysts with the same three supports were also presented as open legends in Fig. 6. Compared to Pt—Cu, Pt catalysts showed better light-off but low selectivity. The order of activity was same as the case of Pt—Cu over 100 °C, i.e. Pt/CeO_2(HSA) > Pt/CeO_2(NT) > Pt/Fe_2O_3, while at 60 °C the Fe_2O_3-supported catalyst showed the highest O_2 conversion, indicating that Fe_2O_3 provides highest oxygen transport ability among monometallic Pt catalysts. The decline of selectivity along

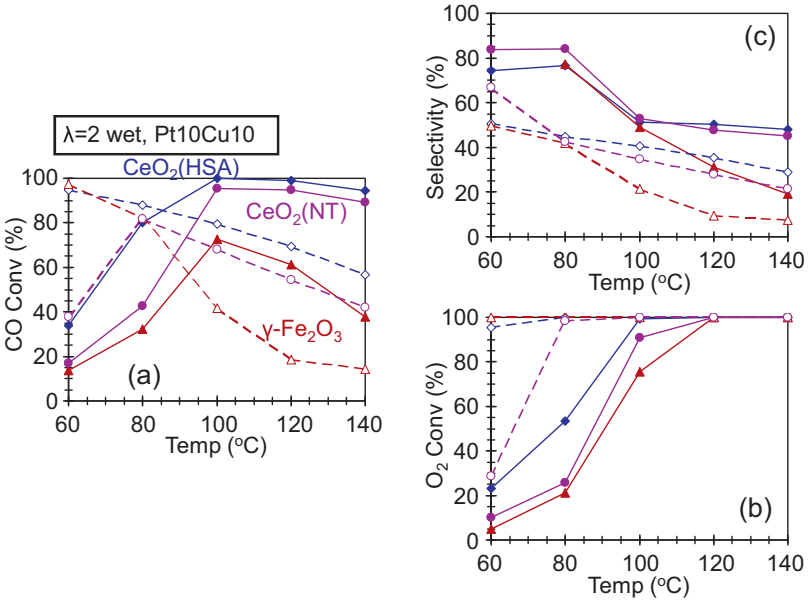

Fig. 6. Effect of support on PROX performance in moisture-added excess O_2/CO condition. The legends are same as in Fig. 5, filled marks: Pt10Cu10 catalysts; open marks: Pt10 catalysts, gas composition: 1% CO/1% O_2/64% H_2/N_2 balance with moisture added by 10% of total gas flow, GHSV = ca. 25,000 h^{-1}.

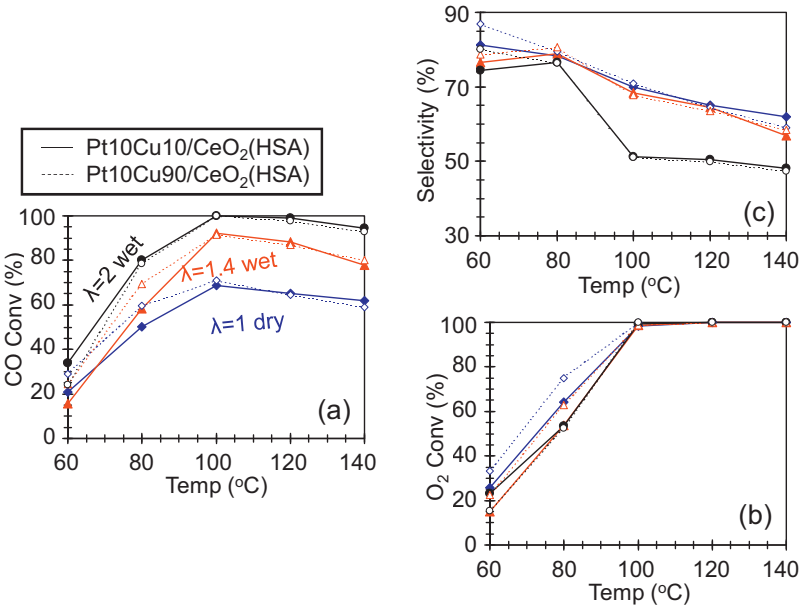

Fig. 7. Effect of O_2/CO ratio and presence of water on PROX performance on Pt—Cu/CeO_2(HSA) catalyst. Filled marks: Pt10Cu10/CeO_2(HSA); open marks: Pt10Cu90/CeO_2(HSA), gas composition: 1% CO/0.5% O_2/67% H_2/N_2 balance (λ = 1 dry, diamond), 1% CO/0.7% O_2/66% H_2/N_2 balance with 10% H_2O (λ = 1.4 wet, triangle), 1% CO/1% O_2/64% H_2/N_2 balance with 10% H_2O (λ = 2 wet, circle). GHSV = ca. 25,000 h^{-1}.

temperature was steepest with Fe_2O_3 support for both monometallic Pt and bimetallic Pt—Cu systems.

In Fig. 7, PROX performances in various λ (O_2/CO ratios) were compared on Pt—Cu/CeO_2(HSA) catalyst. As λ ratio was increased, CO conversion increased while O_2 conversion did not much vary. The oxygen consumption was almost proportional to the O_2 partial pressure in the feed, meaning this sample has high capacity for oxygen adsorption/transport so that activity is ruled by selectivity on this catalyst. Selectivity curves for 1.0 and 1.4 of λ were almost identical, meaning that selectivity is not relevant to O_2 partial pressure but solely dependent on CO coverage. The selectivity drop for 2.0 of λ over 100 °C could be attributed to change in the factor determining selectivity as mentioned earlier.

The reaction characteristics were basically unchanged by the high-Cu Pt10Cu90/CeO_2(HSA) sample (the open legends in Fig. 7). This suggests that most part of CuO species is not much influential, only a small portion of CuO works for catalysis. In our earlier work, on the contrary, CuO content in Pt—Cu/Fe_2O_3 had great impact on activity, which suggests CuO participates in oxygen transport more on Fe_2O_3 than CeO_2 [10].

3.3.2. Comparison of Pt—Cu with monometallic Pt and Cu

To clarify the effect of copper addition to Pt and to compare reaction characteristics in the view point of practical application, the same tests as Fig. 7 were conducted over monometallic Cu/CeO_2 and Pt/CeO_2. Cu/CeO_2 was prepared by impregnation method to achieve 5 wt.% Cu loading that is reported to be optimum for PROX [27]. The results were shown in Fig. 8. Compared with Pt—Cu bimetallic catalyst, Cu/CeO_2 exhibited higher CO conversion in the condition of λ = 1. CO conversion reached 95% at 100 °C, comparable to the value obtained by Kim and Cha [28]. Over 80% of CO conversion was kept up to 160 °C. O_2 conversion was identical to CO conversion below 100 °C (selectivity was 100%) and increase of O_2 partial pressure did not bring any change in CO conversion at all (not shown in Fig. 8), which is consistent with the reported kinetics independent of O_2 partial pressure for this catalyst [29,30]. The reaction is possibly controlled by the number of Cu—O—Ce sites. Only these sites would be able to participate in redox of Cu/CeO_2 [31] in contrast to Pt or Pt—Cu which more strongly interacts with CeO_2 to carry oxygen from wider peripheral area [32] and to alter specific activity of metal surface [33]. For Pt/CeO_2, the presence of both Langmuir–Hinshelwood and Mars and van Krevelen pathways was reported in literature [34].

When 10% moisture was co-present with the excess O_2, the light-off shifted to higher temperature by more than 30 °C, leading to below 20% of CO conversion at 100 °C. CO and O_2 conversions were still identical each other, thus reaction pathway was unchanged. The negative influence of H_2O is attributed to an inhibition of redox at Cu—CeO_2 interface [35]. Since this negative influence was observed only in the co-presence of excessive O_2 and moisture, the active site is not only blocked by H_2O, but also the site itself is chemically changed to inactive one. The wet oxidative condition would change Cu^+ species, which is presumably the active site for PROX [36,37], to Cu^{2+} or hydrated species. This is also confirmed by the observation that CO oxidation reaction in the absence of H_2 was inhibited by moisture more easily in λ = 1 (not shown in figures).

Monometallic Pt exhibited high CO conversion below 80 °C. However, selectivity monotonically decreased along temperature for all the tested conditions. Due to the low selectivity, CO conversion never reached 100% even when O_2 partial pressure was increased.

Comparison among Pt, Pt—Cu and Cu catalysts was made in the condition of λ = 2 with 10% moisture (Fig. 9). Pt—Cu bimetallic catalyst was superior to other two catalysts. Monometallic Pt was more active at low temperature, but it did not work enough at around 100 °C, which is ideal temperature for integrating PROX reactor and fuel cell without a heat exchanger. Cu addition to Pt/CeO_2 significantly improves selectivity though light-off performance below 80 °C was deteriorated. It was demonstrated that CO in H_2-rich gas can be eliminated to less than 50 ppm at 100 °C in the present condition using Pt—Cu bimetallic catalyst. (The detection limit is 20–50 ppm in the present study.) In effort to expand the temperature window for 100% CO conversion, we also prepared Pt/Cu catalyst for which Cu was impregnated and calcined first and Pt was then deposited by electron beam irradiation method. Activity below 100 °C was significantly improved. The Pt/Cu catalyst realized both activity comparable to monometallic Pt and selectivity

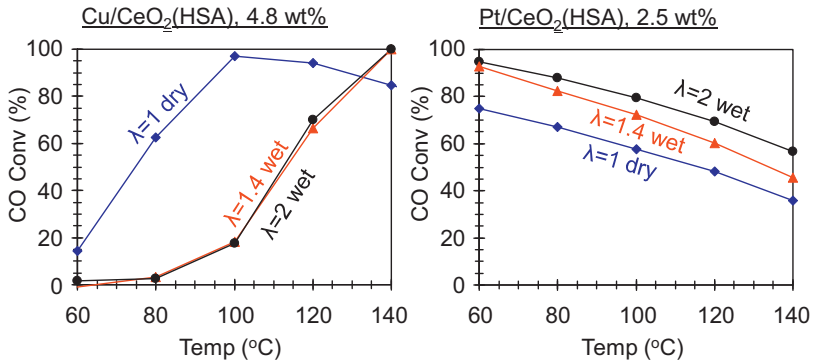

Fig. 8. Effect of O_2/CO ratio and presence of water on PROX activity on monometallic Cu and Pt catalysts. The gas composition and flow rate were same as those in Fig. 7. Pt/CeO_2 was prepared by electron beam irradiation. Cu/CeO_2 was prepared by impregnation method to achieve intended Cu loading.

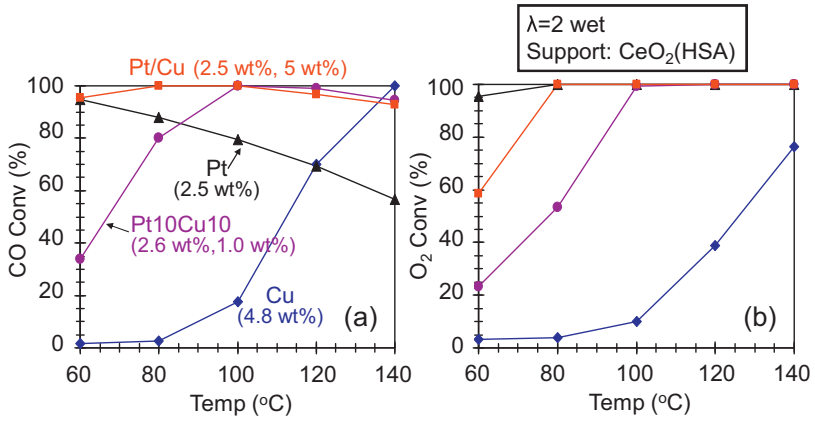

Fig. 9. Comparison of PROX activity between CeO_2-supported Pt—Cu, Cu, and Pt catalysts. Diamond: Cu; triangle: Pt; circle: Pt—Cu; square: Pt/Cu two-step synthesis. The gas composition and flow rate were same as those in Fig. 6.

comparable to bimetallic Pt—Cu. Thus, modification of the structure of Pt—Cu was found effective for improving PROX performance. Relationship between structure and catalytic performance in Pt—Cu is under investigation.

4. Conclusion

Among Pt—M (M = transition metal) bimetallic catalysts supported on CeO_2, Pt—Cu formulation showed uniquely high selectivity in PROX. To investigate the effect of support, Pt—Cu catalysts on various oxide supports were synthesized by electron beam irradiation method. Support material had an influence on both structure of Pt—Cu and reduction behavior of catalyst. Fe_2O_3-supported Pt—Cu showed higher reducibility of CuO species, higher extent of reduction of support, and less Cu incorporation into Pt lattice than CeO_2-supported Pt—Cu, which were attributed to strong interaction of copper with Fe_2O_3 and less interaction of copper with platinum. The catalytic tests showed that Pt—Cu with CeO_2 of small crystallite size had highest activity and selectivity in PROX. O_2 conversion was maintained when O_2 partial pressure was doubled and water vapor was added while other catalysts did not. Such high capacity for oxygen transport was attributed to small CeO_2 crystallite size. CeO_2-supported Pt—Cu also kept high selectivity at low CO coverage region (high CO conversion region) compared to Fe_2O_3-supported catalyst. This made it possible to mitigate CO concentration at the outlet of catalyst bed down to less than 50 ppm at 100 °C in λ = 2 condition. Compared to Pt—Cu/CeO_2, monometallic Cu lost activity when excess O_2 and water vapor coexist in the feed. Monometallic Pt lacked selectivity leading to low CO conversion above 100 °C. Sequential deposition of Pt and Cu on CeO_2 (Cu first by impregnation/calcination and then Pt by electron beam irradiation) further improved low temperature activity of Pt—Cu/CeO_2 system. It realized CO conversion comparable to monometallic Pt below 100 °C while keeping high selectivity of the original Pt—Cu catalyst. Exposed Pt on the surface is thus critical factor for light-off performance.

Acknowledgments

The authors thank K. Ueno (EBIS, Japan) for the provision of beam time of the electron accelerator. The authors also thank Anan Kasei K.K. for providing high surface area CeO_2 support (HSA20). This research was partially supported by the Grant-in-Aid for Scientific Research (No. 22241023) from the Ministry of Education, Culture, Sports, Science and Technology of Japan, the Grant-in-Aid for Young Scientists (A) (No. 22686074) from Japan Society for the Promotion of Science, and R&D Project for Regional Innovation (No. 22U5009) from Ministry of Economy, Trade and Industry.

References

[1] R.A. Lemons, Journal of Power Sources 29 (1990) 251–264.
[2] T.E. Springer, T. Rockward, T.A. Zawodzinski, S. Gottesfeld, Journal of the Electrochemical Society 148 (2001) A11–A23.
[3] L.J. Pettersson, R. Westerholm, International Journal of Hydrogen Energy 26 (2001) 243–264.
[4] M. Kotobuki, A. Watanabe, H. Uchida, H. Yamashita, M. Watanabe, Journal of Catalysis 236 (2005) 262–269.
[5] O.H. Laguna, M.A. Centeno, G. Arzamendi, L.M. Gandia, F. Romero-Sarria, J.A. Odriozola, Catalysis Today 157 (2010) 155–159.
[6] J. Yan, J.X. Ma, P. Cao, P. Li, Catalysis Letters 93 (2004) 55–60.
[7] J. Choi, C.B. Shin, D.J. Suh, Catalysis Communications 9 (2008) 880–885.
[8] T. Komatsu, A. Tamura, Journal of Catalysis 258 (2008) 306–314.

[9] T.A. Yamamoto, T. Nakagawa, S. Seino, H. Nitani, Materials Research Society Symposia Proceedings 1217 (2010) 65–70.
[10] J. Kugai, R. Kitagawa, S. Seino, T. Nakagawa, Y. Ohkubo, H. Nitani, H. Daimon, T.A. Yamamoto, Applied Catalysis A: General 406 (2011) 43–50.
[11] J. Kugai, T. Moriya, S. Seino, T. Nakagawa, Y. Ohkubo, H. Nitani, H. Daimon, T.A. Yamamoto, International Journal of Hydrogen Energy 37 (2012) 4787–4797.
[12] T.S. Mozer, F.B. Passos, International Journal of Hydrogen Energy 36 (2011) 13369–13378.
[13] T.A. Yamamoto, T. Nakagawa, S. Seino, H. Nitani, Applied Catalysis A: General 387 (2010) 195–202.
[14] J. Belloni, M. Mostafavi, in: C.D. Jonah, B.S.M. Rao (Eds.), Radiation Chemistry—Present Status and Future Trends, vol. 87, Elsevier, 2001, pp. 411–452.
[15] S. Seino, T. Kinoshita, T. Nakagawa, T. Kojima, R. Taniguci, S. Okuda, T.A. Yamamoto, Journal of Nanoparticle Research 10 (2008) 1071–1076.
[16] S.K. Jain, E.M. Crabb, L.E. Smart, D. Thompsett, A.M. Steele, Applied Catalysis B: Environmental 89 (2009) 349–355.
[17] E.Y. Ko, E.D. Park, H.C. Lee, D. Lee, S. Kim, Angewandte Chemie International Edition 46 (2007) 734–737.
[18] K.I. Tanaka, M. Shou, H. He, X.Y. Shi, Catalysis Letters 110 (2006) 185–190.
[19] K.I. Tanaka, M. Shou, Y.Z. Yuan, Journal of Physical Chemistry C 114 (2010) 16917–16923.
[20] J. Khatouri, M. Mostafavi, J. Amblard, J. Belloni, Chemical Physics Letters 191 (1992) 351–356.
[21] L. Vegard, Z Physics 5 (1921) 17–26.
[22] W. Liu, M. Flytzani-Stephanopoulos, Chemical Engineering Journal 64 (1996) 283–294.
[23] M.F. Luo, Y.J. Zhong, X.X. Yuan, X.M. Zheng, Applied Catalysis A: General 162 (1997) 121–131.
[24] J. Kugai, J.T. Miller, N. Guo, C. Song, Journal of Catalysis 277 (2011) 46–53.
[25] L. Liu, Z. Yao, B. Liu, L. Dong, Journal of Catalysis 275 (2010) 45–60.
[26] G.S. Zafiris, R.J. Gorte, Journal of Catalysis 143 (1993) 86–91.
[27] G. Avgouropoulos, T. Ioannides, H.K. Matralis, J. Batista, S. Hocevar, Catalysis Letters 73 (2001) 33–40.
[28] D.H. Kim, J.E. Cha, Catalysis Letters 86 (2003) 107–112.
[29] C.D. Baertsch, R. Zhang, T. Haddadin, D.P. Rubiano, H. Nair, C.S. Polster, ACS Catalysis 1 (2011) 519–525.
[30] J.B. Wang, S.C. Lin, T.J. Huang, Applied Catalysis A: General 232 (2002) 107–120.
[31] X.Q. Wang, J.A. Rodriguez, J.C. Hanson, D. Gamarra, A. Martinez-Arias, M. Fernandez-Garcia, Journal of Physical Chemistry B 110 (2006) 428–434.
[32] A. Goguet, F. Meunier, J.P. Breen, R. Burch, M.I. Petch, A.F. Ghenciu, Journal of Catalysis 226 (2004) 382–392.
[33] P. Panagiotopoulou, D.I. Kondarides, Catalysis Today 112 (2006) 49–52.
[34] C.S. Polster, R. Zhang, M.T. Cyb, J.T. Miller, C.D. Baertsch, Journal of Catalysis 273 (2010) 50–58.
[35] C.M. Bae, J.B. Ko, D.H. Kim, Catalysis Communications 6 (2005) 507–511.
[36] H.C. Lee, D.H. Kim, Catalysis Today 132 (2008) 109–116.
[37] R. Kydd, D. Ferri, P. Hug, J. Scott, W.Y. Teoh, R. Amal, Journal of Catalysis 277 (2011) 64–71.